PCCP

PAPER

View Article Online
View Journal | View Issue

Cite this: *Phys. Chem. Chem. Phys.*, 2015, **17**, 1325

Yolk–shell structured $Gd_2O_3:Eu^{3+}$ phosphor prepared by spray pyrolysis: the effect of preparation conditions on microstructure and luminescence properties†

Jung Sang Cho,[a] Kyeong Youl Jung[b] and Yun Chan Kang*[a]

Received 5th August 2014,
Accepted 17th November 2014

DOI: 10.1039/c4cp03477e

www.rsc.org/pccp

$Gd_2O_3:Eu^{3+}$ yolk–shell phosphor powders with high photoluminescence intensity were prepared by spray pyrolysis. Preparation temperature and spray solution concentration were varied to find the optimum process conditions for preparation of $Gd_2O_3:Eu^{3+}$ with yolk–shell structure. The formation mechanism of yolk–shell $Gd_2O_3:Eu^{3+}$ was systematically investigated by observing the microstructures of particles produced under various preparation conditions. The morphological structure of $Gd_2O_3:Eu^{3+}$ powders was clearly dependent on reactor temperature and on the precursor solution concentration. Eventually, pure yolk–shell structured $Gd_2O_3:Eu^{3+}$ powders were obtained for a reaction temperature of 1000 °C and concentration of the spray solution below 0.2 M. Also, the yolk–shell structure formed showed high thermal stability, making it possible to maintain the original spherical yolk–shell structure through calcination at high temperatures. As a result, highly crystalline $Gd_2O_3:Eu^{3+}$ phosphor powders having yolk–shell structure and an agglomeration-free spherical shape were successfully synthesized by spray pyrolysis. These phosphor powders were shown to have good photoluminescence characteristics.

Introduction

There is growing interest in the development of visible light sources for applications in three-dimensional solid-state displays,[1,2] detection of biomolecules,[3,4] two-photon confocal microscopy,[5,6] and white LEDs[7–9] and so on.[10,11] Among the materials used for these applications, rare-earth activated oxide compounds with high-performance luminescence play a key role in producing high-quality end products.[12–18]

The advent of advanced display technologies requires highly photoluminescent phosphors that are thermally stable, exhibit desired emitting colors, and have suitable decay times.[19–21] These properties are generally affected by physical characteristics of the phosphor particles such as particle size, morphology, and crystallinity. Therefore, for phosphor powders, a spherical shape, small particle size with a narrow size distribution, and high crystallinity have been generally considered as chief requirements.[22–24] Basically, luminescence properties of phosphors depend on the type of activators and host composition; a homogeneous distribution of activator ions throughout the host material is needed to obtain high luminescence for advanced display devices.[25] To prepare phosphor powders satisfying the requirements listed above, a number of synthetic approaches such as sol–gel,[26–28] combustion,[29,30] polymer precursor,[31] glycothermal,[32] spray pyrolysis,[33–36] spray drying,[37,38] and hydrothermal methods[39,40] have been investigated. As a result, the powders produced have a wide variety of morphologies, including filled sphere, hollow sphere, nanorod, nanowire, nanoplate, core-shell, tube, and fiber structures.[41–50] Their luminescence properties have been widely investigated.

To obtain high photoluminescence, excitons generated when host materials or activators absorb energy return to the ground state by a radiative process.[51–53] To increase production of excitons, phosphor powders with a morphological structure that maximizes absorption of externally supplied energy can be used.[33] In pursuit of this, the phosphor powders should have a structure with high surface area to effectively harvest the external excitation light. A yolk–shell structure was used for phosphor materials in previous work, and revealed that this could achieve greatly enhanced photoluminescence intensity. The unique yolk–shell structure consists of an inner core, an interstitial hollow space, and an external shell,[54–56] resulting in a high specific surface area and creating potential for yolk–shell materials in phosphors. The enhancement in light absorption in a yolk–shell phosphor powder with a core@void@shell configuration is attributed to

[a] *Department of Materials Science and Engineering, Korea University, Anam-Dong, Seongbuk-Gu, Seoul 136-713, Republic of Korea. E-mail: yckang@korea.ac.kr; Fax: +82-2-928-3584*
[b] *Department of Chemical Engineering, Kongju National University, 1223-24 Cheonan-Daero, Seobuk-gu, Cheonan, Republic of Korea*

† Electronic supplementary information (ESI) available. See DOI: 10.1039/c4cp03477e

multiple light-reflecting and light-scattering in the interstitial void between the core and the shell. In consequence, yolk–shell structures can increase photoluminescence efficiency. Recently, a cost-effective method for large scale production of yolk–shell materials with various compositions was developed.[54,57–60] Kang *et al.* applied liquid droplets formed by a large-scale ultrasonic nebulizer and two-fluid nozzle in the production of yolk–shell materials by simple drying and combustion processes in gas phases.[54,57–59] The developed process can be effectively applied in large scale production of phosphor materials with yolk–shell structure.

In this study, yolk–shell structured Gd_2O_3:Eu powders, which are widely used and serve here as a representative red phosphor material, were synthesized by spray pyrolysis. In a general spray pyrolysis process, a hollow structure with a thin wall is formed when a solute concentration gradient in the droplet is created during evaporation of the droplets in the reactor.[61–64] During this process, solute first precipitates at the more highly supersaturated surface if there is insufficient time for solute diffusion within the droplet. In addition, the gases evolved from decomposition of metal salts lead to formation of a hollow-structured powder. In this work, sucrose was used as the carbon source material to change the drying characteristics of droplets during spray pyrolysis. Polymerization and carbonization of sucrose occur, forming inorganic carbon composites. Subsequently, combustion of the carbon composite is expected to produce the yolk–shell-structured Gd_2O_3:Eu^{3+} phosphor powder. This expected formation mechanism of yolk–shell structured Gd_2O_3:Eu^{3+} powder was elucidated experimentally by changing reaction temperatures and noting the resulting morphological changes. In addition, the effect of the spray solution concentration on morphology was investigated.

Experimental

Sample preparation

Yolk–shell structured Gd_2O_3:Eu^{3+} phosphor powders were synthesized by ultrasonic spray pyrolysis. A schematic illustration of the ultrasonic spray pyrolysis system used for the synthesis is shown in Fig. S1 in the ESI.† The spray pyrolysis apparatus consisted of an ultrasonic aerosol generator with six 1.7 MHz resonators to generate droplets, a quartz reactor (1200 mm in length and 50 mm in inner diameter), and a Teflon bag filter. Reactor temperatures of 400, 600, 800, and 1000 °C were used. The flow rate of air used as carrier gas in the reactor was fixed at 10 L min^{-1}. Gadolinium oxide (Gd_2O_3, 99.9%, Rhodia) and europium oxide (Eu_2O_3, 99.9%, Aldrich) were used as source materials of the Gd and Eu components, respectively. For the synthesis of the powders, spray solutions were prepared by dissolving gadolinium oxide (Gd_2O_3, 99.9%, Rhodia) and europium oxide (Eu_2O_3, 99.9%, Aldrich) into 1 L of deionized water containing nitric acid (60%; Aldrich). The total concentrations of Gd and Eu elements were changed to be 0.05, 0.2, and 1.0 M. The mole fraction of Eu, Eu/(Eu + Gd) was fixed at 0.125 in all the spray solutions. The amount of Gd_2O_3, Eu_2O_3, and nitric acid for the spray solution of 0.2 M was 31.7, 4.4, and 12.0 g, respectively. Next, 0.5 M of sucrose ($C_{12}H_{22}O_{11}$, Junsei) as the carbon source material for preparation of the yolk–shell Gd_2O_3:Eu^{3+} powders was added into the above solutions. The as-prepared powders were post-treated in a box furnace at temperatures between 900 and 1200 °C for 3 h under an air atmosphere.

Characterization

Microstructures of the powders were observed by scanning electron microscopy (SEM) (JSM-6060, JEOL) and field-emission transmission electron microscopy (FETEM) (JEM-2100F, JEOL). Crystal phases of the powders were evaluated by X-ray diffractometry (XRD) (X'Pert PRO MPD, Philips) using Cu K_α radiation (λ = 1.5418 Å) at the Korea Basic Science Institute (Daegu). Surface areas of the powders were measured by the Brunauer–Emmett–Teller (BET) method using N_2 as an adsorbate gas. Photoluminescence spectra were measured using a spectrophotometer (LS 50, Perkin Elmer) with a Xe flash lamp as the excitation light source. Thermogravimetric (TG) analysis was performed simultaneously using a thermogravimetric analyzer (Pyris 1 TGA, Perkin Elmer) in the temperature range of 25–600 °C, at a heating rate of 10 °C min^{-1} under a static air atmosphere. An image analyzer (ImageJ, NIH) was used to determine particle-size distributions of the powders.

Results and discussion

Morphologies of the $Gd_{1.88}O_3$:$Eu_{0.12}$ phosphor powders prepared at various temperatures by spray pyrolysis from the solutions with sucrose are shown in Fig. 1. The powder particles had spherical shapes and did not show aggregation, irrespective of preparation temperature. However, with an increase in the preparation temperature, mean particle size decreased. The mean particle sizes estimated from SEM results were 1.2, 1.0, 0.8, and 0.6 μm for preparation temperatures of 400, 600, 800, and 1000 °C, respectively. The combustion degree of carbon component and densification according to the preparation temperatures

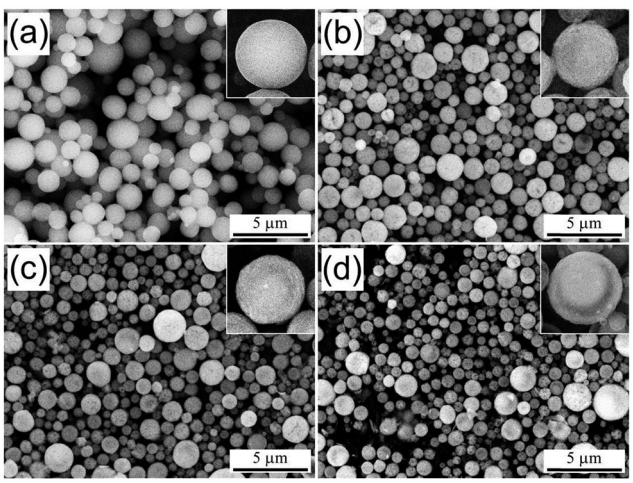

Fig. 1 SEM images of the as-prepared Gd_2O_3:Eu^{3+} phosphor powders prepared at the temperature of (a) 400 °C, (b) 600 °C, (c) 800 °C, and (d) 1000 °C.

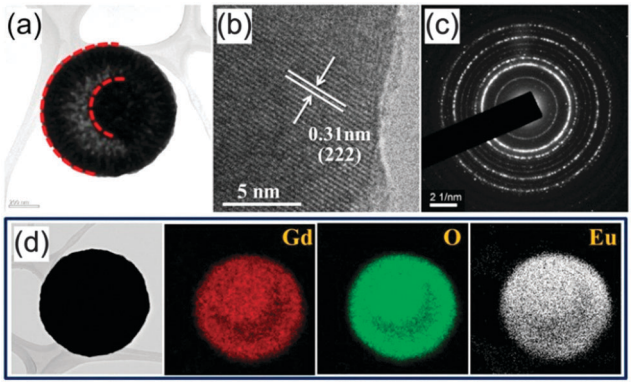

Fig. 2 Morphologies and elemental mapping images of the as-prepared Gd_2O_3:Eu^{3+} phosphor powders prepared at the temperature of 1000 °C: (a) TEM image of the powder, (b) HR-TEM image of the powder, (c) SAED pattern of the powder, and (d) dot-mapping images of the powder.

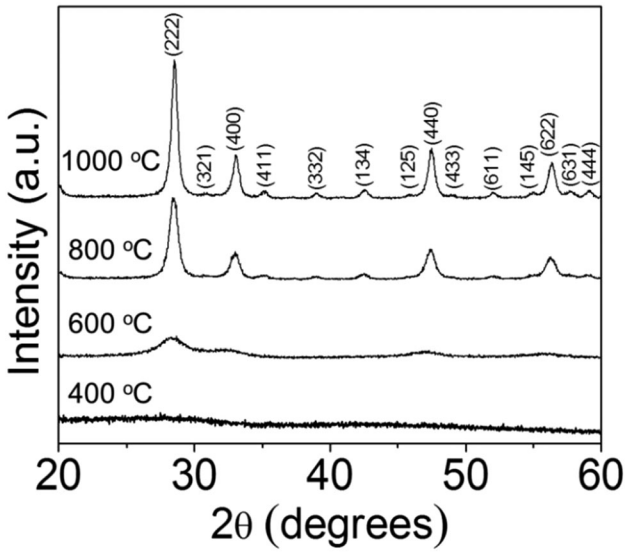

Fig. 3 XRD patterns of the as-prepared Gd_2O_3:Eu phosphor powders prepared at the various reaction temperatures.

changed the mean size of the particles. From the inset images of the powders, yolk–shell structure was perceptible for the specimens prepared at 800 °C and 1000 °C (Fig. 1c and d). For preparation temperatures of 400 °C and 600 °C, the powders have a filled rather than a yolk–shell structure.

More-detailed microstructures of the as-prepared Gd_2O_3:Eu^{3+} phosphor powders prepared at 1000 °C were observed by TEM and elemental mapping images are shown in Fig. 2. In Fig. 2a, the powders show the yolk–shell structure with a configuration of external shell, inside core, and interstitial hollow space. The core, with submicron dimensions, is located inside a hollow shell having a thickness of several tens of nanometers. The high-resolution TEM image in Fig. 2b shows clear lattice fringes separated by 0.31 nm, corresponding to the (222) plane of Gd_2O_3:Eu^{3+} (JCPDS Card No. 43-1014). In addition, in the corresponding selected-area electron diffraction (SAED) pattern in Fig. 2c, well-defined concentric rings indicate that the powder obtained at 1000 °C has a polycrystalline Gd_2O_3 phase with high crystallinity. All ingredients in droplets can be mixed well in a molecular level, which makes it possible to achieve the uniform substitution of Eu ions into host lattices. To check this, an elemental mapping was carried out. The mapping results shown in Fig. 2d indicate that europium activators are uniformly distributed over the Gd_2O_3 host matrix. This demonstrates that no phase separation of the components occurs in the drying and decomposition processes of the droplets.

In order to investigate the effect of preparation temperature on the phase and structure of the as-prepared Gd_2O_3:Eu^{3+} particles, XRD analysis was carried out; the results are displayed in Fig. 3. For particles prepared at 400 °C, no diffraction peaks corresponding to the crystalline form of Gd_2O_3 are observed. This indicates that a purely thermal decomposition of the precursors followed by Gd_2O_3 crystallization did not occur, and the powders prepared at 400 °C consist of a carbon composite containing gadolinium and europium components. The existence of carbon components was identified by TG analysis, shown in Fig. S2a (ESI†): gradual weight loss was observed up to approximately 650 °C, and is due to decomposition of residual elementary carbon and metal salts in the composite structure. Total weight loss was 46%. In the specimen prepared at 600 °C, low, broad peaks assigned to the cubic phase of Gd_2O_3 are observed, indicating that crystallization to the Gd_2O_3 phase occurs at the surface of powders. The XRD peak intensity steadily increased and the peak became narrower with increased preparation temperature. From the TG results shown in Fig. S2(a) (ESI†), it can be seen that during the heating cycle, there was no weight loss for temperatures above 650 °C. That is, decomposition of Gd, Eu, and carbon components is complete at this temperature. For the phosphor sample prepared at 1000 °C, no weight loss was observed (see Fig. S2(b), ESI†), and it is concluded that carbon components were entirely decomposed and highly crystalline Gd_2O_3 powders produced. The mean crystallite sizes, calculated by the Scherrer equation from the (222)-reflection peak widths in the XRD patterns, were 4.2, 10.6, and 16.5 nm for preparation temperatures of 600, 800, and 1000 °C, respectively. This increase in crystallite size indicates that crystallinity of the as-prepared Gd_2O_3:Eu^{3+} phosphor powders increases with increasing preparation temperature.

From the above results for different preparation temperatures, the formation mechanism of yolk–shell Gd_2O_3:Eu^{3+} phosphor powders can be summarized: at 400 °C, the lowest preparation temperature studied, spherical powders with a filled structure were formed instead of a yolk–shell structure as seen in Fig. 1a. The carbon source, sucrose, is not fully decomposed due to the low reaction temperature, and an intermediate product composed of gadolinium, europium, and carbon compounds results. At higher preparation temperatures, surface combustion of the carbon forms composite particles having a core–shell structure (core: C–Gd–Eu–O/shell: Gd_2O_3:Eu). Given that the Gd_2O_3 cubic phase was observed at 600 °C (Fig. 3), the surface combustion generates a crystallized Gd_2O_3 shell. Subsequently, the contraction of the C–Gd–Eu core as a result of further heating leads to formation of yolk–shell powders (C–Gd–Eu–O@void@Gd_2O_3:Eu). Finally, at the highest preparation temperature of 1000 °C studied,

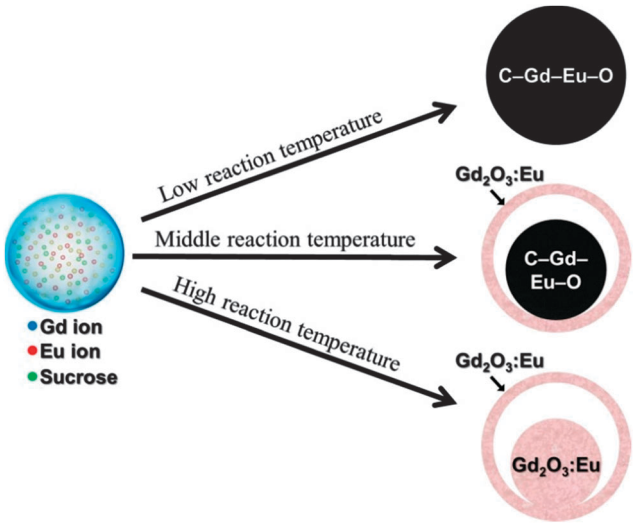

Scheme 1 Schematic diagram of the different Gd_2O_3:Eu^{3+} morphologies of each powder created by different preparation temperatures.

thermal decomposition of the core produces yolk–shell Gd_2O_3:Eu^{3+} phosphor powder with the Gd_2O_3:Eu@void@Gd_2O_3:Eu configuration. Rapid combustion of the carbon component elevates the powder temperature during formation of the yolk–shell structure. Therefore, the activation of Eu^{3+} (substitution of Eu^{3+} into the Gd_2O_3 host) takes place simultaneously with crystallization of the amorphous phase during formation of the yolk–shell structure, and results in Gd_2O_3:Eu^{3+} phosphor powder. The generation of a yolk–shell structure was confirmed by SEM (Fig. 1d) and TEM (Fig. 2) observations. TG analysis (Fig. S2, ESI†) verified the complete decomposition of residual carbon during formation of a yolk–shell structure, and production of a pure Gd_2O_3:Eu phase was confirmed by XRD (Fig. 3). The structures observed for different preparation temperatures are summarized in Scheme 1.

The concentration of the starting spray solution can affect the morphology of the Gd_2O_3:Eu^{3+} phosphor powder particles. To investigate this, the total concentration of the Gd and Eu components was varied from 0.05 M up to 1.0 M. Fig. 4 shows SEM images of powders prepared at a reactor temperature of 1000 °C. For spray solution concentrations of 0.05 M and 0.2 M, the resulting powders showed identical yolk–shell structures (Fig. 1(d)). However, powders prepared from 1.0 M solution showed a large thin walled hollow sphere (Fig. 4(b)). The mean particle size of particles prepared at 0.05 M was about 0.49 μm, smaller than that (0.64 μm) at 0.2 M. For a salt concentration of 1.0 M, the mean particle size was about 3.4 μm. In spray pyrolysis, particle size (d_p) depends on the salt concentration (C) as: $d_p \propto C^{1/3}$. Then, the particle sizes at 0.2 M and 1.0 M should theoretically be about 1.6 and 2.7 times that at 0.05 M, respectively. The ratios of measured particle sizes at these concentrations to those at 0.05 M were about 1.3 and 6.9, respectively. In a yolk–shell structure, however, observed particle size strongly depends on the void fraction or the outer-shell thickness. Given this, the size ratio between two samples prepared at 0.05 and 0.2 M is reasonable. However, the measured average particle size for 1.0 M is much larger than expected from the theoretical relation: $d_p \propto C^{1/3}$, as a result of

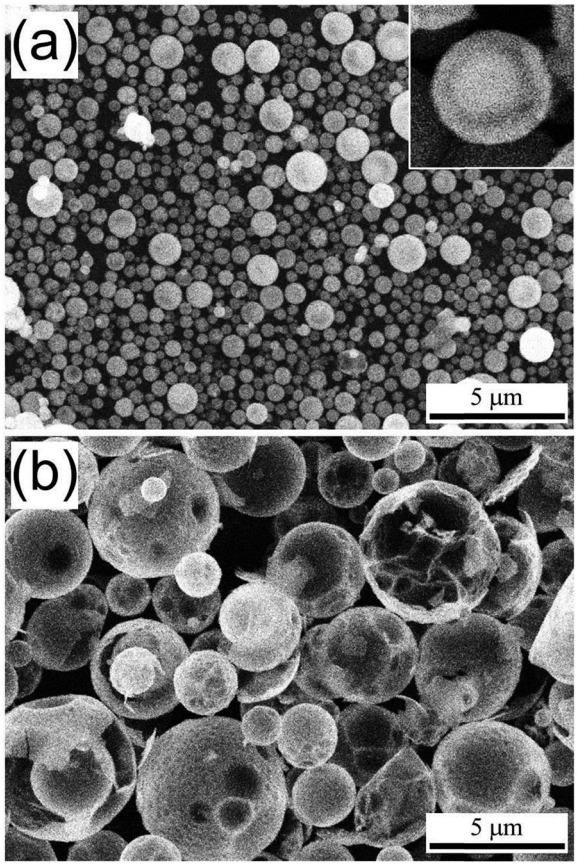

Fig. 4 SEM images of the Gd_2O_3:Eu phosphor powders prepared at different concentration of spray solution at 1000 °C: (a) 0.05 M, (b) 1.0 M.

the hollow-structure. Generation of hollow-structured particles at 1.0 M can be explained by the following arguments. In this work, the concentration of sucrose was fixed although the Gd and Eu concentration was varied from 0.05 M to 1.0 M. Therefore, sucrose cannot change the drying characteristics of the droplets. In contrast, the high concentration of salts in the spray solution can change where precipitation of salts occurs in the droplets. When the initial salt concentration is low, the polymerization of sucrose first occurs before the surface concentration of salts in droplets reaches the critical saturation. As a result, volumetric precipitation is the dominant process in the generation of carbon–inorganic composite particles with a filled morphology. On the other hand, when the initial salt concentration is high, the surface concentration of salts can reach supersaturation when even a small fraction of water has been evaporated. Thus, the surface precipitation of salts begins with the polymerization of sucrose, and consecutively a carbon–salt shell is inflated like a balloon by the elevated pressure inside droplets due to evaporated water or gases evolved from precursor decomposition. Subsequently, hollow-structured precipitates (carbon–inorganic composite) formed are thermally decomposed, generating hollow Gd_2O_3:Eu^{3+} particles. From these results, the concentration of a spray solution is critical in determining the morphology of Gd_2O_3:Eu^{3+} powders. On the basis of the results achieved so far, the process conditions to obtain yolk–shell structured

$Gd_2O_3:Eu^{3+}$ powders *via* a one-pot spray process were a reactor temperature of 1000 °C and a solution concentration of 0.2 M or lower.

To increase crystallinity and activate the Eu ions for powders having yolk–shell structure, the powders obtained at 1000 °C were post heat-treated at various temperatures. In the literature on the $Gd_2O_3:Eu^{3+}$ phosphor, high photoluminescence was achieved for a post treatment process at around 1000 °C.[42,46,47] For this investigation, the prepared powders were post heat-treated at temperatures between 900 and 1200 °C; Fig. 5 shows TEM images of the $Gd_2O_3:Eu^{3+}$ phosphor particles processed at various temperatures. All specimens have a yolk–shell structure after the post thermal treatment. Additionally, no agglomeration between particles occurs, maintaining the spherical shape regardless of the thermal treatment temperatures. However, with an increase in the heat treatment temperature, the grain size of the particle also increases (Fig. S3, ESI†). The specific surface areas of the post heat-treated powder are 5.1, 4.8, 2.4 and 1.3 $m^2\ g^{-1}$ for powders post treated at 900, 1000, 1100 and 1200 °C, respectively, as shown in Fig. S4 (ESI†). The decrements in specific surface area indicate that more densification occurs with increasing post treatment temperature.

XRD analysis was conducted in order to confirm the relation of phase and crystallite size to post heat treatment temperatures. As shown in Fig. 6, the major crystal phase was cubic, regardless of thermal treatment temperature. For a temperature of 1200 °C, the monoclinic phase was detected as an impurity phase. That is, at 1200 °C, some cubic phase was transformed into monoclinic.[65,66] The crystallite sizes of the cubic phase were calculated by the Scherrer equation from peak widths of the (222)-reflection in the XRD patterns. The resulting crystallite sizes were 31, 48, 95, and 132 nm for temperatures of 900, 1000, 1100, and 1200 °C, respectively.

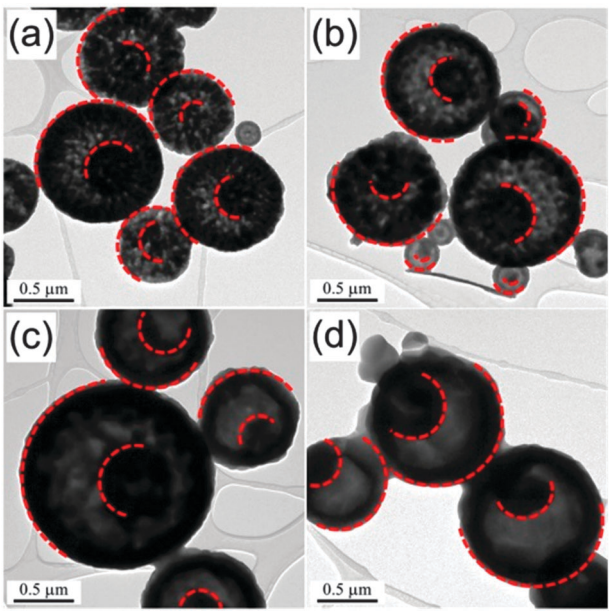

Fig. 5 TEM images of the post heat-treated $Gd_2O_3:Eu^{3+}$ phosphor powders prepared at the temperature of 1000 °C: (a) 900 °C, (b) 1000 °C, (c) 1100 °C, and (d) 1200 °C.

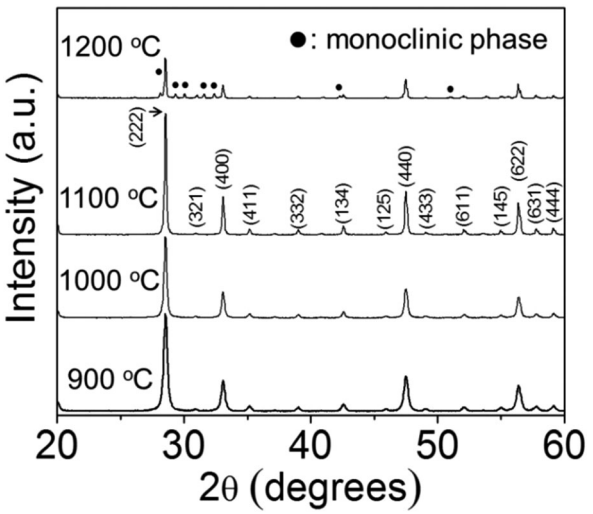

Fig. 6 XRD patterns of the post-treated $Gd_2O_3:Eu^{3+}$ phosphor powders at the various temperatures.

The increments in crystallite sizes are in good agreement with the TEM results shown in Fig. 5 and Fig. S3 (ESI†).

Fig. 7 shows the photoluminescence properties of the yolk–shell structured $Gd_2O_3:Eu^{3+}$ phosphor powders post treated at various temperatures. The emission spectra were observed using excitation by 254 nm ultraviolet (UV) light; luminescence was measured at the main emission peak of 612 nm. It is well known that cubic phase $Gd_2O_3:Eu^{3+}$ phosphor absorbs UV light through a charge transfer band (CTB) process and the 612 nm red emission is due to the $^5D_0$–$^7F_2$ transition in Eu^{3+} ions.[43] The excitation band centered at 248 nm is attributed to CTB absorption between O^{2-} and Eu^{3+}. For the internal transition ($^8S \rightarrow {}^6P$) of Gd^{3+} and the $^4f_6$ intra-configurational transition of Eu^{3+}, the excitation intensities were very weak. To elucidate the existence of internal transitions, the enlarged spectrum in wavelength regions longer than 300 nm for the sample post-treated at 1100 °C was shown in the inset of Fig. 7(a). The peak at 314 nm was due to the $^8S \rightarrow {}^6P$ transition of Gd^{3+} ions. Above 350 nm, all peaks observed were due to the f–f transition of Eu^{3+}. In the yolk–shell $Gd_2O_3:Eu^{3+}$ phosphor, the most intense absorption band was corresponding to the $O^{2-} \rightarrow Eu^{3+}$ energy transfer. Fig. 7(b) shows the emission spectra of yolk–shell structured $Gd_2O_3:Eu^{3+}$. The red emission observed matches the luminescence characteristics of $Gd_2O_3:Eu^{3+}$ phosphor. The emission spectrum of cubic Gd_2O_3:Eu displays $^5D_0$–^7F_J (J = 0, 1, 2, 3, 4) transitions typical of Eu^{3+} ions. The strongest emission peak, centered at 612 nm, is due to the $^5D_0$–$^7F_2$ transition of Eu^{3+} ions. The emission intensity of the $Gd_2O_3:Eu^{3+}$ yolk–shell phosphor powders increases with increasing post-treatment temperature up to 1100 °C. In general, the luminescence intensity of phosphors can be enhanced by increasing the crystallinity.[19,34,35] Under the assumption that there is no significant difference in particle size, smaller surface area yields higher emission intensity because of a decreased number of surface defects. The BET, XRD, and TEM results indicate that crystallinity was increased and the surface area was reduced progressively by increasing

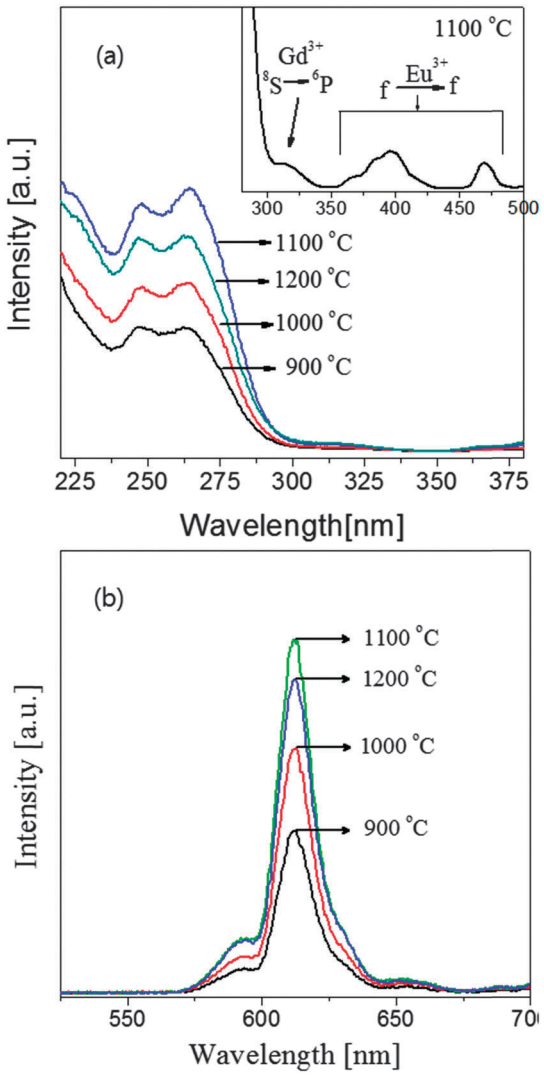

Fig. 7 Photoluminescence (a) excitation, and (b) emission spectra of the Gd_2O_3:Eu^{3+} phosphor powders at the various sintering temperatures.

the calcination temperature. Given these results, the emission intensity should monotonically increase with increasing post heat treatment temperature. However, the highest emission intensity was achieved at 1100 °C. The crystal phase is a crucial factor influencing the emission properties of phosphors. For a Gd_2O_3:Eu^{3+} phosphor, the cubic phase is known to have better luminescence characteristics compared to monoclinic.[65,66] Therefore, despite the larger crystallite size and smaller surface area for the powder thermally treated at 1200 °C compared to that treated at 1100 °C, the relatively lower emission intensity at 1200 °C results from the presence of the monoclinic phase as an impurity. The optimal thermal treatment temperature for yolk–shell structured Gd_2O_3:Eu^{3+} phosphor to have its highest photoluminescence was determined to be 1100 °C.

Conclusions

In this study, the yolk–shell structured Gd_2O_3:Eu^{3+} was prepared by spray pyrolysis and the particle formation mechanism was systematically examined by controlling the preparation temperature and concentration of the spray solution. The microstructures of Gd_2O_3:Eu^{3+} particles were strongly influenced by the reactor temperature as well as the precursor concentration. To prepare Gd_2O_3:Eu^{3+} particles having a yolk–shell structure, the reactor temperature should be higher than 600 °C and the concentration of precursor salts should be lower than 0.2 M. Pure yolk–shell structured Gd_2O_3:Eu^{3+} can be directly produced at a reaction temperature of 1000 °C because residual carbon remaining in the powder is entirely decomposed at this temperature. The yolk–shell structure of Gd_2O_3:Eu^{3+} particles showed good thermal stability in that no agglomeration was observed after post heat treatment in the temperature range from 900 °C to 1200 °C. The highest photoluminescence intensity of Gd_2O_3:Eu^{3+} yolk–shell powder was obtained with a post-treatment temperature of 1100 °C. The spray pyrolysis technology developed in this study is expected to be widely applicable to the preparation of yolk–shell structured phosphor powders with enhanced photoluminescence intensity.

Acknowledgements

This work was supported by the National Research Foundation of Korea (NRF) grant funded by the Korea government (MEST) (No. 2012R1A2A2A02046367).

Notes and references

1 M. Gately, Y. Zhai, M. Yeary, E. Petrich and L. Sawalha, *J. Disp. Technol.*, 2011, **7**, 503.
2 N. S. Holliman, N. A. Dodgson, G. E. Favalora and L. Pockett, *IEEE Trans. Broadcast.*, 2011, **57**, 362.
3 D. Tu, W. Zheng, Y. Liu, H. Zhu and X. Chen, *Coord. Chem. Rev.*, 2014, **273**, 13.
4 Y. Wang, L. Bao, Z. Liu and D. W. Pang, *Anal. Chem.*, 2011, **83**, 8130.
5 N. N. Dong, M. Pedroni, F. Piccinelli, G. Conti, A. Sbarbati, J. E. Ramírez-Hernández, L. M. Maestro, M. C. Iglesias-de la Cruz, F. Sanz-Rodriguez, A. Juarranz, F. Chen, F. Vetrone, J. A. Capobianco, J. G. Sole, M. Bettinelli, D. Jaque and A. Speghini, *ACS Nano*, 2011, **5**, 8665.
6 J. Pichaandi, J. C. Boyer, K. R. Delaney and F. C. J. M. Van Veggel, *J. Phys. Chem. C*, 2011, **115**, 19054.
7 D. S. Kang, H. S. Yoo, S. H. Jung, H. K. Kim and D. Y. Jeon, *J. Phys. Chem. C*, 2011, **115**, 24334.
8 V. Kumar, A. Bedyal, J. Sharma, V. Kumar, O. Ntwaeaborwa and H. Swart, *Appl. Phys. A: Mater. Sci. Process.*, 2014, **116**, 1785.
9 P. Pust, V. Weiler, C. Hecht, A. Tücks, A. S. Wochnik, A. K. Henß, D. Wiechert, C. Scheu, P. J. Schmidt and W. Schnick, *Nat. Mater.*, 2014, **13**, 891.
10 D. Gedamu, I. Paulowicz, S. Kaps, O. Lupan, S. Wille, G. Haidarschin, Y. K. Mishra and R. Adelung, *Adv. Mater.*, 2014, **26**, 1541.
11 T. Reimer, I. Paulowicz, R. Röder, S. Kaps, O. Lupan, S. Chemnitz, W. Benecke, C. Ronning, R. Adelung and Y. K. Mishra, *ACS Appl. Mater. Interfaces*, 2014, **6**, 7806.

12 M. Ganapathi, S. V. Eliseeva, N. R. Brooks, D. Soccol, J. Fransaer and K. Binnemans, *J. Mater. Chem.*, 2012, **22**, 5514.
13 A. S. Gouveia Neto, A. F. Da Silva, L. A. Bueno and E. B. Da Costa, *J. Lumin.*, 2012, **132**, 299.
14 Y. C. Kang, H. S. Roh, S. B. Park and H. D. Park, *J. Eur. Ceram. Soc.*, 2002, **22**, 1661.
15 V. Kumar, V. Kumar, S. Som, M. M. Duvenhage, O. M. Ntwaeaborwa and H. C. Swart, *Appl. Surf. Sci.*, 2014, **308**, 419.
16 S. Som, A. K. Kunti, V. Kumar, V. Kumar, S. Dutta, M. Chowdhury, S. K. Sharma, J. J. Terblans and H. C. Swart, *J. Appl. Phys.*, 2014, **115**, 193101.
17 S. Som, P. Mitra, V. Kumar, V. Kumar, J. J. Terblans, H. C. Swart and S. K. Sharma, *Dalton Trans.*, 2014, **43**, 9860.
18 Y. Xu, W. Yang, X. Li, W. Li and X. Ju, *Luminescence*, 2014, **29**, 711.
19 T. Igarashi, M. Ihara, T. Kusunoki, K. Ohno, T. Isobe and M. Senna, *Appl. Phys. Lett.*, 2000, **76**, 1549.
20 Y. C. Kang, I. W. Lenggoro, S. B. Park and K. Okuyama, *J. Solid State Chem.*, 1999, **146**, 168.
21 Y. C. Kang and H. D. Park, *Appl. Phys. A: Mater. Sci. Process.*, 2003, **77**, 529.
22 N. Joffin, B. Caillier, J. Dexpert Ghys, M. Verelst, G. Baret, A. Garcia, P. Guillot, J. Galy, R. Mauricot and S. Schamm, *J. Phys. D: Appl. Phys.*, 2005, **38**, 3261.
23 Y. C. Kang, H. S. Roh, S. B. Park and K. Y. Jung, *Jpn. J. Appl. Phys.*, 2004, **43**, 5302.
24 C. Panatarani, I. Wuled Lenggoro and K. Okuyama, *J. Phys. Chem. Solids*, 2004, **65**, 1843.
25 D. Zhao, X. Li, R. Wang and F. Zhang, *Nano Lett.*, 2014, **14**, 3634.
26 J. Liao, H. You, D. Zhou, H. r. Wen and R. Hong, *Opt. Mater.*, 2012, **34**, 1468.
27 H. Wu, Y. Hu, W. Zhang, F. Kang, N. Li and G. Ju, *J. Sol-Gel Sci. Technol.*, 2012, **62**, 227.
28 Y. Xie, L. J. Xiao, F. Q. Yan, Y. J. Chen, W. Z. Li and X. J. Geng, *J. Nanosci. Nanotechnol.*, 2014, **14**, 4486.
29 F. Hong, L. Zhou, L. Li, Q. Xia and X. Luo, *Opt. Commun.*, 2014, **316**, 206.
30 J. T. Ingle, R. P. Sonekar, S. K. Omanwar, Y. Wang and L. Zhao, *Combust. Sci. Technol.*, 2014, **186**, 83.
31 K. Su, T. D. Tilley and M. J. Sailor, *J. Am. Chem. Soc.*, 1996, **118**, 3459.
32 K. Uegaito, S. Hosokawa and M. Inoue, *J. Lumin.*, 2012, **132**, 64.
33 J. S. Cho, K. M. Yang and Y. C. Kang, *CrystEngComm*, 2014, **16**, 6170.
34 Y. C. Kang, S. B. Park, I. W. Lenggoro and K. Okuyama, *J. Electrochem. Soc.*, 1999, **146**, 2744.
35 Y. C. Kang, H. S. Roh and S. B. Park, *Adv. Mater.*, 2000, **12**, 451.
36 Y. C. Kang, H. S. Roh and S. B. Park, *J. Am. Ceram. Soc.*, 2001, **84**, 447.
37 T. Han, S. Cao, D. Zhu, C. Zhao, M. Ma, M. Tu and J. Zhang, *Optik*, 2013, **124**, 3539.
38 A. Nakamura, N. Nambu and H. Saitoh, *Sci. Technol. Adv. Mater.*, 2005, **6**, 210.
39 J. Wan, Z. Wang, X. Chen, L. Mu, W. Yu and Y. Qian, *J. Lumin.*, 2006, **121**, 32.
40 J. H. Zeng, H. L. Fu, T. J. Lou, Y. Yu, Y. H. Sun and D. Y. Li, *Mater. Res. Bull.*, 2009, **44**, 1106.
41 A. Bao, H. Lai, Y. Yang, W. Xu, C. Tao, H. Zhang and H. Yang, *J. Cryst. Growth*, 2008, **310**, 4394.
42 E. M. Goldys, K. Drozdowicz Tomsia, S. Jinjun, D. Dosev, I. M. Kennedy, S. Yatsunenko and M. Godlewski, *J. Am. Chem. Soc.*, 2006, **128**, 14498.
43 G. Jia, K. Liu, Y. Zheng, Y. Song, M. Yang and H. You, *J. Phys. Chem. C*, 2009, **113**, 6050.
44 G. Jia, H. You, K. Liu, Y. Zheng, N. Guo and H. Zhang, *Langmuir*, 2009, **26**, 5122.
45 K. M. Lin and Y. Y. Li, *Nanotechnology*, 2006, **17**, 4048.
46 Y. Liu, P. Yang, W. Wang, H. Dong and J. Lin, *CrystEngComm*, 2010, **12**, 3717.
47 M. Nichkova, D. Dosev, S. J. Gee, B. D. Hammock and I. M. Kennedy, *Anal. Chem.*, 2005, **77**, 6864.
48 R. S. Ningthoujam, L. R. Singh, V. Sudarsan and S. Dorendrajit Singh, *J. Alloys Compd.*, 2009, **484**, 782.
49 J. Wang, Y. Xu, M. Hojamberdiev, J. Peng and G. Zhu, *Mater. Sci. Eng., B*, 2009, **156**, 42.
50 J. Yang, C. Li, Z. Cheng, X. Zhang, Z. Quan, C. Zhang and J. Lin, *J. Phys. Chem. C*, 2007, **111**, 18148.
51 H. F. Brito, J. Hölsä, T. Laamanen, M. Lastusaari, M. Malkamäki and L. C. Rodrigues, *Opt. Mater. Express*, 2012, **2**, 371.
52 X. Chen, J. Zhao, L. Yu, C. Rong, C. Li and S. Lian, *J. Lumin.*, 2011, **131**, 2697.
53 L. C. V. Rodrigues, H. F. Brito, J. Hölsä, R. Stefani, M. C. F. C. Felinto, M. Lastusaari, T. Laamanen and L. A. O. Nunes, *J. Phys. Chem. C*, 2012, **116**, 11232.
54 Y. J. Hong, M. Y. Son and Y. C. Kang, *Adv. Mater.*, 2013, **25**, 2279.
55 J. Liu, Y. Zhou, J. Wang, Y. Pan and D. Xue, *Chem. Commun.*, 2011, **47**, 10380.
56 N. Liu, H. Wu, M. T. McDowell, Y. Yao, C. Wang and Y. Cui, *Nano Lett.*, 2012, **12**, 3315.
57 J. S. Cho and Y. C. Kang, *RSC Adv.*, 2014, **4**, 25234.
58 J. S. Cho, J. H. Lee and Y. C. Kang, *Phys. Chem. Chem. Phys.*, 2014, **16**, 16962.
59 S. H. Choi and Y. C. Kang, *Chem. – Eur. J.*, 2014, **20**, 5835.
60 H. Gao, G. Wang, Y. Luan, K. Chaikittikul, X. Zhang, M. Yang, W. Dong and Z. Shi, *CrystEngComm*, 2014, **16**, 2520.
61 J. S. Cho, Y. N. Ko, H. Y. Koo and Y. C. Kang, *J. Mater. Sci.: Mater. Med.*, 2010, **21**, 1143.
62 J. S. Cho and S. H. Rhee, *J. Eur. Ceram. Soc.*, 2013, **33**, 233.
63 D. S. Jung, S. B. Park and Y. C. Kang, *Korean J. Chem. Eng.*, 2010, **27**, 1621.
64 J. H. Yi, J. H. Kim, H. Y. Koo, Y. N. Ko, Y. C. Kang and J. H. Lee, *J. Power Sources*, 2011, **196**, 2858.
65 Y. Iwako, Y. Akimoto, M. Omiya, T. Ueda and T. Yokomori, *J. Lumin.*, 2010, **130**, 1470.
66 G. Xia, S. Wang, S. Zhou and J. Xu, *Nanotechnology*, 2010, **21**, 345601.